Luminescent Supramolecular Ionic Frameworks based on Organic Fluorescent Polycations and poly Anionic Phosphorescent Metal Clusters

Ilya Kashnik, Binying Yang, Spartak Yarovoi, Taisiya Sukhikh, Marie Cordier, Grégory Taupier, Konstantin Brylev, Pierre-Antoine Bouit, Yann Molard

Chemistry–A European Journal
Research Article
doi.org/10.1002/chem.202400079
Chemistry Europe
European Chemical Societies Publishing
www.chemeurj.org

Luminescent Supramolecular Ionic Frameworks based on Organic Fluorescent Polycations and Polyanionic Phosphorescent Metal Clusters

Ilya V. Kashnik,[a, b] Binying Yang,[b] Spartak S. Yarovoi,[a] Taisiya S. Sukhikh,[a] Marie Cordier,[b] Grégory Taupier,[b] Konstantin A. Brylev,[a] Pierre-Antoine Bouit,*[b] and Yann Molard*[b]

Emissive ionic supramolecular frameworks are designed by associating tetraphenylethylene-based tetra-cationic units and di-anionic molybdenum or tetra-anionic rhenium octahedral clusters. Obtained structures were characterized by single-crystal X-ray diffraction. The emission properties of the hybrids were investigated as dry powders or in various solvents by one photon and two photon absorption leading to a O_2 concentration dependent luminescence color for the Mo based hybrid.

Introduction

Smart hybrid materials made of organic and inorganic building blocks are versatile materials which properties depend not only on the intrinsic features of the isolated components but also on cooperative effects occurring between them. They have drawn an increasing attention for their potential in applications in a tremendous amount of fields among which electronic, housing, energy, optics, health and diagnosis …[1] Getting and keeping a good homogeneity between the organic and inorganic phases or molecular components within the composite is fundamental to preserve their functionalities for long-term applications. Several types of strong and/or weak interactions have been used or combined to do so: covalent linking using sol-gel techniques, coordination bonds, or supramolecular interactions like hydrogen bonds or host-guest systems.[2] In all these cases the assembly is driven by the directionality of the interactions which allows to predict, to some extent, the final structuration of the targeted hybrid. For this reason, relying only on non-directional electrostatic interactions to build an organic-inorganic framework or a so-called ionic crystal, starting from molecular functional components, is particularly rare and challenging. It involves polyionic (at least di-ionic) species of opposite charge which pairing will insure the supramolecular organization. Rare examples are based on charged coordination cages[3] or Polyoxometalates (POMs)[4] for which the versatility of their architectures and charges, combined to the possibility of using bulky macrocations such as cationic metal complexes or functionalized porphyrins have led to porous ionic crystals further used for heterogenous catalysis, selective adsorption of guests,[5] or for electrocatalytic hydrogen evolution reaction.[6] However, these materials are either difficult to prepare because of tedious procedures or they call on long reaction time or high temperature like solvothermal or hydrothermal synthesis. On the other hand, luminescent frameworks based on emissive cations or Aggregation Induced Emission (AIE) -active luminophores have focus the attention of many research groups because of their potential applications in optoelectronics, sensors or photovoltaics.[7] As a classical AIE emitter, tetraphenylethylene (TPE, Figure 1) derivatives are very attractive building blocks to generate Supramolecular or Metal Organic Frameworks (SOF or MOF, respectively) and design materials with chemical sensing abilities, solid-state emissive materials or bioprobes,[7d] as they display intense luminescence in the condense phase. Indeed, TPEs are easy to synthesize and functionalize.[8] Among the plethora of possible functionalizations, introducing one or several cationic heads such as

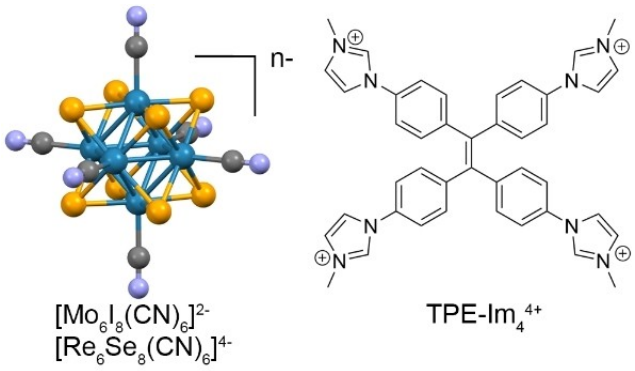

Figure 1. Representation of the inorganic (colors: blue – Mo or Re metal atoms, orange – I or Se, grey – carbon, pale blue – nitrogen) (left) and organic (right) polyionic emissive building blocks associated to generate SOF.

[a] I. V. Kashnik, Dr. S. S. Yarovoi, Dr. T. S. Sukhikh, Prof. K. A. Brylev
Nikolaev Institute of Inorganic Chemistry SB RAS
3 Acad. Lavrentiev ave., 630090 Novosibirsk, Russian Federation
[b] I. V. Kashnik, B. Yang, M. Cordier, Dr. G. Taupier, Dr. P.-A. Bouit, Prof. Y. Molard
Université de Rennes, CNRS, ISCR – UMR 6226, ScanMAT – UAR 2025
F-35000 Rennes, France
E-mail: yann.molard@univ-rennes.fr
pierre-antoine.bouit@univ-rennes.fr

Supporting information for this article is available on the WWW under https://doi.org/10.1002/chem.202400079

ammonium, imidazolium, guanidinium or pyridinium generally leads to blue emissive materials.[9] However, despite all possible associations, polycationic TPEs have never been associated to polyanionic entities to design ionic supramolecular frameworks. Indeed, TPEs functionalized with one ammonium head were recently associated to LnW_{10} and P_2W_{18} POMs leading to 2D assemblies.[10] A bisammonium TPE derivative was intercalated into layered α-zirconium phosphate nanosheets, leading to hybrid materials showing a strong blue emissions.[11]

Here, we present the first supramolecular ionic frameworks based on a tetracationic TPE and either a dianionic octahedral molybdenum cluster complex or a tetraanionic octahedral rhenium cluster complex. Such frameworks are easily obtained at 25 °C by mixing the two precursor solutions. Octahedral metal cluster compounds of general formula $A_n[M_6L^i_8L^a_6]$ (A = alkali cation, M = transition metal; L^i = inner ligand; L^a = apical ligand, see Figure 1), are maintained by metal-metal bonds.[12] The metallic scaffold M_6 is covalently bonded to eight face-capping ligands (μ_3-L^i) and is stabilized by six apical ones (L^a). When the hexametallic scaffold is made of molybdenum or rhenium atoms, such metal cluster compounds can be highly red-NIR phosphorescent[13] with excited state lifetimes in the range of several tens or even hundreds of microseconds.[14] They show an unrivalled photostability[15] and a very large Stokes shift.[16] As a real alternative to rare earth or precious metal cations emitting in the same area (Eu^{3+}, Pt^{2+}, Ir^{3+}, Pd^{2+} or Ru^{2+}), they have been integrated in soft nanocomposites without modification of their emission abilities.[17] The triplet excited state of M_6 clusters also reacts efficiently with O_2.[18] This ability allows their use as O_2 sensor devices[19] or as theranostic tool in photodynamic therapy.[13,20] Surprisingly, although M_6 clusters have been associated with a large variety of organic monocations, up to now, only one research group associated $[Re_6Q_8(CN)_6]^{4-}$ (Q = S or Se) with a non-emissive bisamidinium cation, giving a network in which the stabilization is mainly driven by H-bonds.[21] Here, we also used a $[Mo_6I_8(CN)_6]^{2-}$ dianion that was never integrated in hybrid organic-inorganic compounds. Although such clusters do not display the highest luminescence efficiencies (*vide infra*), they have been chosen for a proof of concept as both of them bear six CN apical ligands. Hence, we expect that only the influence of the cluster charge will impact on the final supramolecular assembly.

Results and Discussion

The tetraimidazolium salt **[TPE-Im$_4$]I$_4$** was obtained by the methylation of the corresponding imidazole[22] with iodomethane in a hot DMF solution (Figure S1). Mixing **[TPE-Im$_4$]I$_4$** at 25 °C with $Cs_4[Re_6Se_8(CN)_6]\cdot 3H_2O$[21] or $Cs_{1.3}Na_{0.7}[Mo_6I_8(CN)_6]\cdot 2H_2O$[23] (further noted **Cs$_4$Re**, or **A$_2$Mo**, respectively) in a methanol or methanol/water mixture leads to a cationic metathesis and immediate precipitation of **[TPE-Im$_4$][Re$_6$Se$_8$(CN)$_6$]** (**TPE-Re**) or **[TPE-Im$_4$][Mo$_6$I$_8$(CN)$_6$]$_2$** (**TPE-Mo**) respectively, as powders. These hybrids are insoluble in any common solvents. Only a poor solubility in hot DMF for **TPE-Re** or in DMSO for **TPE-Mo** allowed the formation of single crystals suitable for X-Ray data collection and characterization by ^{1}H NMR spectroscopy for the latter case. Compared to **[TPE-Im$_4$]I$_4$**, the electrostatic interactions between **[TPE-Im$_4$]$^{4+}$** and **[Mo$_6$I$_8$(CN)$_6$]$^{2-}$** lead to a slight upfield shift of proton signals beard by the imidazolium heads and to the broadening of proton signals belonging to the phenyl rings due to the hampering of their rotation (see Figures S2–S4 for NMR spectra).

According to the single-crystal X-ray diffraction analysis (SCXRD),[24] **TPE-Re** consists of compact layers in which the **[TPE-Im$_4$]$^{4+}$** cations alternate with anionic cluster units forming zigzag chains (Figure 2a). Each **[Re$_6$Se$_8$(CN)$_6$]$^{4-}$** cluster is surrounded by 4 cations and vice versa, leading to a 1:1 stoichiometry. No short contact interactions are found between the cluster units. CN apical ligands are in short contacts with proton or carbon atoms belonging to **[TPE-Im$_4$]$^{4+}$** while two Se inner ligands located in *trans*-position are in short contact with carbon atoms from phenyl rings (Figure S5). These interactions maintain the phenyl rings quasi perpendicular to the plan of the double bond with a torsion angle value of 88.24°, prohibiting any photocyclization process in the solid state.[25] The arrangement of these layers leads to the formation of voids forming 2D-channels with a calculated volume of 0.134 $cm^3 g^{-1}$ occupied by disordered solvent molecules. For **TPE-Mo**, 2D-channels are also found in the single crystal structure with a calculated volume of 0.122 $cm^3 g^{-1}$ occupied also by disordered solvent molecules. The hybrid organizes in alternate plans of **[Mo$_6$I$_8$(CN)$_6$]$^{2-}$** and **[TPE-Im$_4$]$^{4+}$**. Interactions (short contacts) are found between adjacent clusters and between inner or apical ligands of the anion and **[TPE-Im$_4$]$^{4+}$** (Figures S6–S7). The phenyl rings are not perpendicular to the double bond plane

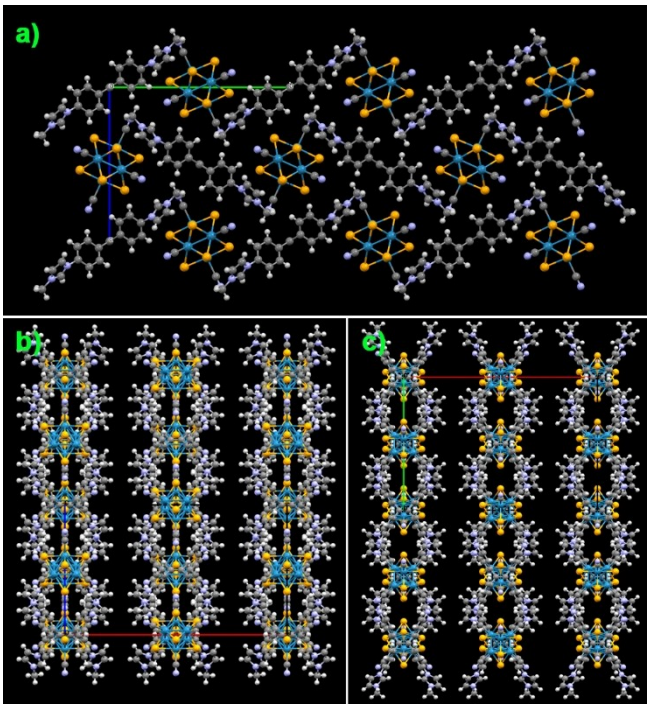

Figure 2. Representation according to SCXRD of **TPE-Re**; a) along a axis; b) along b axis and c) along c axis.

but photocyclization is unlikely considering the torsion angle values that lie between 111.52° and 136.47°.[25] Attempts by varying concentrations of the metal clusters and/or **[TPE-Im$_4$]I$_4$** solutions lead always to hybrids with the same structure geometry.

Thermogravimetric analysis was performed on both hybrids and starting compounds to assess their thermal stability (Figures S8–S10 for thermograms). **[TPE-Im$_4$]I$_4$** started to decompose only at ~300 °C, while both cluster precursors are stable up to ~500 °C. Heating **TPE-Mo** from 27 °C induces a progressive weight loss going up to 8% at ~300 °C and corresponding to the removal of solvent molecules. This loss is followed by the decomposition of **[TPE-Im$_4$]$^{4+}$** at higher temperature. Surprisingly, for **TPE-Re**, the thermal stability of **[TPE-Im$_4$]$^{4+}$** is largely enhanced. Its thermogram contains a first weight loss of 9% ending around 190 °C that corresponds to the loss of solvent molecules trapped within the pores. This loss is followed by a plateau up to around 390 °C when **[TPE-Im$_4$]$^{4+}$** starts to degrade. Hence, powder X-ray diffraction (PXRD) experiments were realized before and after heating the two hybrids under dynamic vacuum at 5 °C min^{-1} to observe the influence of solvent molecule loss on the hybrid structural integrity: it appears that at 125 °C the structure of **TPE-Mo** collapses, *i.e.* way before the complete loss of solvent molecules, while **TPE-Re** still shows crystallinity even when heated at 250 °C. However, a slight shift to higher angle values is observed on the diffraction signal maxima of the diffractogram compared to the theoretical one deduced from SCXRD, meaning a shortening of inter-cluster distances induced by the solvent molecule loss (see Figures S11–S12 for PXRD patterns). The initial **TPE-Re** crystallinity could be partially recovered by soaking the powder in DMF for 24 h at 25 °C. Using other polar solvents like acetone, acetonitrile or water did not affect the structure of **TPE-Re** observed after drying, giving hints about an excellent stability in the solid state with a possible loss of porosity. This loss of porosity after thermal treatment was further confirmed by gas adsorption measurements which indicated a low porosity of 11.5 m^2 g^{-1} with a type 2 N_2 adsorption isotherm (Figure S13). Soaking **TPE-Re** in apolar solvents like toluene and pentane however induced a partial to complete amorphization of the material.

We then investigated the photophysical properties of precursors and hybrids by steady state and time dependent studies in the solid state and in solution when possible. Similarly to previous reports, **[TPE-Im$_4$]I$_4$** absorbs in the UV.[22] **A$_2$Mo** and **Cs$_4$Re** display absorptions in the UV that tail in the visible (Figures S14–S16), and show a typical red-NIR broad phosphorescence either in solution or in the solid state with emission maxima at around 675 and 713 nm, respectively, upon excitation in the UV-2A range. On the other hand, emission properties of TPE derivatives being dependent on the phenyl ring torsional rigidity,[26] **[TPE-Im$_4$]I$_4$** practically does not emit in solution. The luminescence in solution is not turned on when the measurement is performed at 77 K, which discard the conformational flexibility from being the cause of the low quantum yield. As expected, it exhibits a typical blue fluorescence with a maximum at 490 nm in the solid state with an average lifetime of 1.8 ns, in the range of known TPE derivatives.[7g] Surprisingly, its absolute emission quantum yield was estimated at 1%, which is considerably lower than related analogs previously described.[22] As the absorption spectra of **[Mo$_6$I$_8$(CN)$_6$]$^{2-}$** and **[Re$_6$Se$_8$(CN)$_6$]$^{4-}$** overlap partially the emission signal of **[TPE-Im$_4$]$^{4+}$** (Figures S14–S18), energy transfers from the organic emitter to the inorganic ones are expected. Indeed, Förster radius of 2.3 or 2.4 nm were calculated between **[TPE-Im$_4$]$^{4+}$** and **[Mo$_6$I$_8$(CN)$_6$]$^{2-}$** or **[Re$_6$Se$_8$(CN)$_6$]$^{4-}$**, respectively. Photophysical parameters are gathered in Table 1, while emission spectra observed by one-photon or two-photon absorption (1PA or 2PA, respectively) are presented in Figure 3 (See ESI Figures S19–S28 for all other related photophysical data).

In hybrid powders, the blue emission characteristic of the organic fluorescent cation disappears completely and only the NIR cluster related emission band remains, together with an increase of the emission lifetime component and the enhancement of the quantum yield for **TPE-Re**. This confirms an efficient energy transfer from the TPE moieties to the metal clusters. Surprisingly, the **[TPE-Im$_4$]$^{4+}$** emission is much more noticeable when **TPE-Re** powder is soaked in various aerated solvents or when **TPE-Mo** is solubilized in DMSO (Figure 3b).

In solution, this phenomenon could be imparted to two factors: i) the hindering of the phenyl-imidazolium rotation induced by the electrostatic interactions with the polyanionic clusters and ii) the quenching of cluster phosphorescence induced by dissolved O_2.

For **TPE-Re**, while the dry sample emits in the deep red region with CIE 1931 color coordinates of x = 0.69 and y = 0.29, soaking it in various solvents does not affect dramatically the global emission envelop leading to a red-orange emission. For **TPE-Mo**, its solubilization enhances its O_2 emission quenching

Table 1. Photophysical data in the solid state and in deaerated solvent deduced from steady state and time dependent photoluminescence measurements at λ_{exc} = 375 nm: emission maxima (λ_{max}), excited states lifetime (τ_i) with corresponding amplitude (a_i), average lifetime (τ_{av}) and absolute quantum yield (Φ).

Sample	λ_{max}/ nm	τ_1/(a_1)	τ_2/(a_2)	τ_3/(a_3)	τ_{av} [a]	Φ/%
[TPE-Im$_4$]I$_4$ powder	490	0.2 ns (87%)	0.8 ns (10%)	4.4 ns (3%)	1.8 ns	1
A$_2$Mo powder	673	1.2 µs (86%)	3.8 µs (14%)	–	2.1 µs	1
A$_2$Mo in DMSO	677	84 µs	–	–	84 µs	22
TPE-Mo powder	674	1.1 µs (57%)	4.7 µs (43%)	–	3.8 µs	1
TPE-Mo in DMSO	673	14 µs (49%)	45 µs (51%)	–	38 µs	6
Cs$_4$Re powder	713	1.5 µs (57%)	4.0 µs (43%)	–	3.2 µs	5
TPE-Re powder	713	3.1 µs (39%)	8.9 µs (61%)	–	7.8 µs	7

[a] Average lifetime is calculated as $\tau = (\Sigma a_i \tau_i^2)/(\Sigma a_i \tau_i)$.

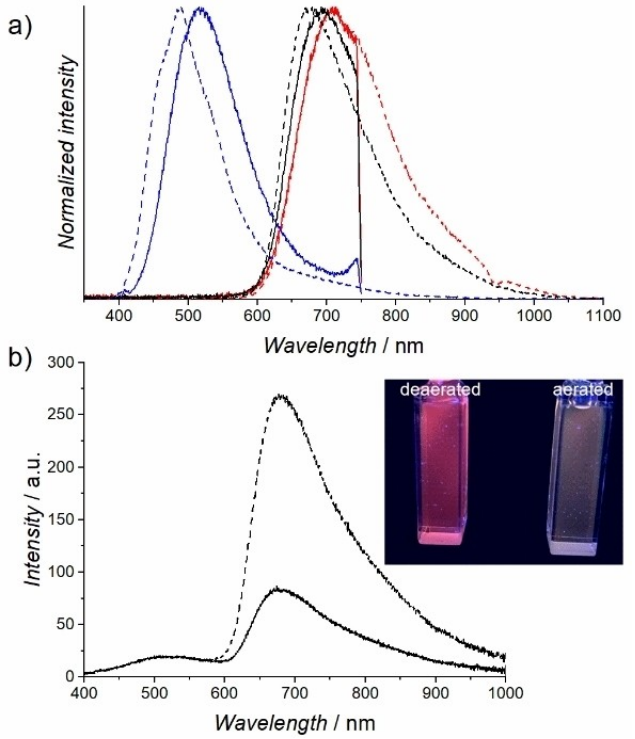

Figure 3. Emission of a) [**TPE-Im$_4$**]I_4 (blue), **TPE-Re** (red) and **TPE-Mo** (black) in the solid state by 1PA (λ_{exc} = 375 nm, dashed line) and 2PA (λ_{exc} = 820 nm, solid line, short-pass filter at 750 nm), b) **TPE-Mo** in aerated (solid line) and deaerated (dashed line) DMSO; inset: corresponding solutions under UV-2A irradiation.

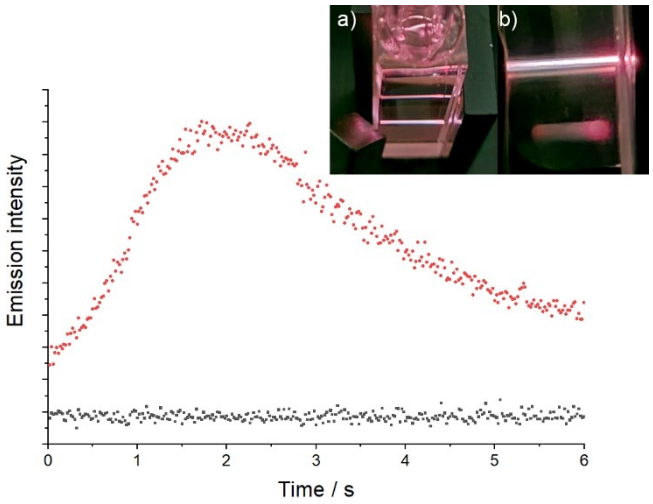

Figure 4. Follow up of the emission intensity vs irradiation time of **TPE-Mo** in aerated DMSO (λ_{exc} = 375 nm, integration time 20 ms) at 505 nm (black dots) and 692 nm (red dots); inset a) picture of the quartz cell containing the solution upon excitation and b) zoom of the laser beam pathway. The traces at the bottom is the reflection of the emission signal on an optical filter placed behind.

efficiency which deeply impacts on the emission color. As shown in the inset of Figure 3b, **TPE-Mo** passes, upon deaeration, from a white emission (x = 0.42 and y = 0.37) to an orange-pink one (x = 0.53 and y = 0.34) (see Figure S29 for the CIE diagram). We also noticed serendipitously the same change of color, but to a less extent, when the aerated solution was irradiated long enough with the 375 nm pulsed laser used for lifetime measurements. Upon constant irradiation, the emission color of the aerated solution evolves all along the laser beam (inset a and b in Figure 4): the white emission appears more reddish at the edges of the quartz cell and the red emission is guided within the cell walls. This phenomenon is very similar to what we previously observed when $[Mo_6I_8(OCOC_2F_5)_6]^{2-}$ was associated to a blue-green emissive oxindole derivative in polymer matrices.[27] It can be explained by a slight variation of the 375 nm photon density along the laser beam which induces a little modulation of the local O_2 concentration in the solution due to its consumption by reaction with the excited triplet state of the cluster complex. First, the laser beam crosses the quartz cell wall and enters the solution at full power with a high photon density as it has not been absorbed yet. In the middle of the solution, due to the partial absorption of the excitation signal, the laser beam photon density decreases a little. Finally, when the laser beam reaches the opposite cell wall, part of it is reflected orthogonally which locally increases slightly the photon density, and again causes a lowering of the local O_2 concentration due to singlet oxygen (O_2 $^1\Delta_g$) production. Such observation highlights the high sensitivity of our hybrids toward oxygen and demonstrates that they could be used as oxygen sensor once the emission properties of both organic and inorganic building blocks will be optimized in terms of emission efficiency.

Hence, this result pushes us to investigate the emission behavior of the **TPE-Mo** solution under constant irradiation by recording emission spectra on a timescale of 20 ms using a CCD based spectrometer. Figure 4 presents the evolution of the emission intensity at 505 and 692 nm with the irradiation time. While the TPE emission band intensity does not vary, we observed a large increase of the cluster emission intensity during the two first seconds of irradiation (due to the decrease of O_2 concentration at the edges of the laser beam within the cell), followed by a decrease and a stabilization. A possible explanation of this observation would be that, initially, the laser beam induces, locally on its path, a slight increase of the temperature which leads to the appearance of a convection flow within the solution. Let us stress that recorded emission spectra are in fact an average of what is observed in the cell, and, stirring the solution leads again to a homogeneous white emission all along the laser beam that quickly evolves to the previous situation without stirring.

The production of singlet oxygen (O_2 $^1\Delta_g$) by **TPE-Mo** could be evidenced upon irradiation in the solid state at 375 nm by looking at the appearance of its emission in the near infrared area at 1270 nm (see ESI Figure S30). Such production is highly relevant for biological applications such as photodynamic therapy and many groups, including our, are investigating this promising alternative solution against cancer.[28] However, red-NIR excitation is preferred during such treatment as UV-2A excitation does not penetrate deeply human tissues and can cause damages. Hence, we first investigated the emission abilities of our hybrids by a two-photon absorption process at

$\lambda_{exc} = 820$ nm which was demonstrated by the quadratic relation found between the emission intensity and the excitation power, either in the solid state or in solution (see Figures S31–S34). Emission spectra are perfectly superimposable with those observed by 1PA for the cluster emission range. For TPE, a red shift of the emission maximum from 490 up to 530 nm is observed. For **A_2Mo** and **TPE-Mo**, 2PA cross section values could be estimated in DMSO using Rhodamine B as reference,[29] for excitation ranging from 810 up to 900 nm and are in the range of previously reported values for clusters (lower than 1 GM on the all studied excitation range), without any particular enhancement for the hybrid compared to the cluster alone.[30]

Conclusions

To summarize, we present herein the first ionically assembled emissive supramolecular frameworks obtained by associating two model compounds: polyanionic red-NIR emitting octahedral metal clusters ($[Mo_6I_8(CN)_6]^{2-}$ or $[Re_6Se_8(CN)_6]^{4-}$) and an organic AIEgen tetracation (**$[TPE\text{-}Im_4]^{4+}$**). Hybrids are easily obtained by precipitation upon mixing the precursor salt solutions at 25 °C. According to SCXRD, hybrids self-arrange into porous architectures. **TPE-Mo** shows a more pronounced molecular character as it can be solubilized in DMSO while the electrostatic interactions strongly bind **$[Re_6Se_8(CN)_6]^{4-}$** with **$[TPE\text{-}Im_4]^{4+}$** leading to a hybrid with an enhanced thermal stability compared to the organic compound alone. Indeed, drying hybrids at 250 °C leads to the amorphization of **TPE-Mo** and to the loss of **TPE-Re** porosity. For the latter, the initial structure could be recovered partially upon soaking in DMF, and soaking in other polar solvent like water, acetonitrile or acetone, did not modify its structure, illustrating its excellent chemical stability. Luminescence properties evaluated in the solid state show the complete disappearance of the TPE emission signal and an enhancement of the cluster emission lifetime, characteristic of an efficient energy transfer between the emitters. Solubilizing **TPE-Mo** in DMSO leads to a white emission that turns to the orange-pink upon deaeration. This color change is also observed when a 375 nm laser beam constantly irradiates its aerated solution which demonstrates its high sensitivity against O_2 concentration. Emission properties by 2PA are very similar to the one observed by 1PA. While model compounds (either organic or inorganic) do not display optimized luminescence properties, their assembly show promising perspectives toward the design of emissive supramolecular ionic frameworks using optimized luminescent cations/anions tandems. Such systems will be reported shortly.

Supporting Information

The authors have cited additional references within the Supporting Information[31]

Acknowledgements

Authors acknowledge ISCR and Dr. S. Cordier for financial support through the interéquipe projects and the CLUSPOM IRP Network, respectively. Authors thank Dr. F. Tessier for BET measurements. I. V. K. thanks the French Embassy for providing the Vernadski scholarship for the co-tutelle PhD program between France and Russia. I. V. K. and K. A. B. thank Russian science foundation (project 19-73-20196-p).

Conflict of Interests

The authors declare no conflict of interest.

Data Availability Statement

The data that support the findings of this study are available from the corresponding author upon reasonable request.

Keywords: Metal Organic Framework · luminescence · metal cluster · supramolecular chemistry

[1] a) C. Sanchez, P. Belleville, M. Popall, L. Nicole, *Chem. Soc. Rev.* **2011**, *40*, 696–753; b) S. Parola, B. Julián-López, L. D. Carlos, C. Sanchez, *Adv. Funct. Mater.* **2016**, *26*, 6506–6544.
[2] a) K. Dey, S. Mohata, R. Banerjee, *ACS Nano* **2021**, *15*, 12723–12740; b) J. Tian, Z.-Y. Xu, D.-W. Zhang, H. Wang, S.-H. Xie, D.-W. Xu, Y.-H. Ren, H. Wang, Y. Liu, Z.-T. Li, *Nat. Commun.* **2016**, *7*, 11580; c) G. Zhang, B. Li, Y. Zhou, X. Chen, B. Li, Z.-Y. Lu, L. Wu, *Nat. Commun.* **2020**, *11*, 425; d) S. Dutta, Y. D. More, S. Fajal, W. Mandal, G. K. Dam, S. K. Ghosh, *Chem. Commun.* **2022**, *58*, 13676–13698; e) W. Fang, Z. Mu, Y. He, K. Kong, K. Jiang, R. Tang, Z. Liu, *Nature* **2023**, *619*, 293–299; f) X. Chen, R.-K. Huang, K. Takahashi, S.-i. Noro, T. Nakamura, I. Hisaki, *Angew. Chem. Int. Ed.* **2022**, *61*, e202211686; g) Z.-T. Li, S.-B. Yu, Y. Liu, J. Tian, D.-W. Zhang, *Acc. Chem. Res.* **2022**, *55*, 2316–2325; h) C. Sanchez, G. J. d. A. A. Soler-Illia, F. Ribot, T. Lalot, C. R. Mayer, V. Cabuil, *Chem. Mater.* **2001**, *13*, 3061–3083; i) S. L. James, *Chem. Soc. Rev.* **2003**, *32*, 276–288.
[3] a) A. J. Gosselin, G. E. Decker, A. M. Antonio, G. R. Lorzing, G. P. A. Yap, E. D. Bloch, *J. Am. Chem. Soc.* **2020**, *142*, 9594–9598; b) N. Jackson, I. R. Vazquez, Y.-P. Chen, Y.-S. Chen, W.-Y. Gao, *Chem. Commun.* **2021**, *57*, 7248–7251.
[4] a) B. Nohra, H. El Moll, L. M. Rodriguez Albelo, P. Mialane, J. Marrot, C. Mellot-Draznieks, M. O'Keeffe, R. Ngo Biboum, J. Lemaire, B. Keita, L. Nadjo, A. Dolbecq, *J. Am. Chem. Soc.* **2011**, *133*, 13363–13374; b) C. Streb, C. Ritchie, D.-L. Long, P. Kögerler, L. Cronin, *Angew. Chem. Int. Ed.* **2007**, *46*, 7579–7582.
[5] Y. Zhang, Y. Liu, D. Wang, J. Liu, J. Zhao, L. Chen, *Polyoxometalates* **2023**, *2*, 9140017.
[6] D. Zang, Z. Huo, S. Yang, Q. Li, G. Dai, M. Zeng, L. Ruhlmann, Y. Wei, *Mater. Today Commun.* **2022**, *31*, 103811.
[7] a) M. D. Allendorf, C. A. Bauer, R. K. Bhakta, R. J. T. Houk, *Chem. Soc. Rev.* **2009**, *38*, 1330–1352; b) J. Rocha, L. D. Carlos, F. A. A. Paz, D. Ananias, *Chem. Soc. Rev.* **2011**, *40*, 926–940; c) W. P. Lustig, S. Mukherjee, N. D. Rudd, A. V. Desai, J. Li, S. K. Ghosh, *Chem. Soc. Rev.* **2017**, *46*, 3242–3285; d) J. Mei, N. L. C. Leung, R. T. K. Kwok, J. W. Y. Lam, B. Z. Tang, *Chem. Rev.* **2015**, *115*; e) Y. Wen, T. Sheng, X. Zhu, C. Zhuo, S. Su, H. Li, S. Hu, Q.-L. Zhu, X. Wu, *Adv. Mater.* **2017**, *29*, 1700778; f) Y. Su, J. Yu, Y. Li, S. F. Z. Phua, G. Liu, W. Q. Lim, X. Yang, R. Ganguly, C. Dang, C. Yang, Y. Zhao, *Chem. Commun.* **2018**, *1*, 12; g) X. He, H. Bi, P. Wei, *J. Mater. Chem. C* **2023**, *11*, 3675–3691.
[8] D. D. La, S. V. Bhosale, L. A. Jones, S. V. Bhosale, *ACS Appl. Mater. Interfaces* **2018**, *10*, 12189–12216.

[9] J. Knelles, S. Beardsworth, K. Bader, J. R. Bruckner, A. Bühlmeyer, R. Forschner, K. Schweizer, W. Frey, F. Giesselmann, Y. Molard, S. Laschat, *ChemPhysChem* **2019**, *20*, 2210–2216.
[10] S. Rong, M. Wang, X. Wang, *Angew. Chem. Int. Ed.* **2023**, *62*, e202310018.
[11] D. Li, C. Miao, X. Wang, X. Yu, J. Yu, R. Xu, *Chem. Commun.* **2013**, *49*, 9549–9551.
[12] F. A. Cotton, *Inorg. Chem.* **1964**, *3*, 1217–1220.
[13] K. Kirakci, P. Kubat, M. Dusek, K. Fejfarova, V. Sicha, J. Mosinger, K. Lang, *Eur. J. Inorg. Chem.* **2012**, *2012*, 3107–3111.
[14] a) A. W. Maverick, H. B. Gray, *J. Am. Chem. Soc.* **1981**, *103*, 1298–1300; b) M. A. Mikhaylov, M. N. Sokolov, *Eur. J. Inorg. Chem.* **2019**, *2019*, 4181–4197.
[15] M. Amela-Cortes, Y. Molard, S. Paofai, A. Desert, J.-L. Duvail, N. G. Naumov, S. Cordier, *Dalton Trans.* **2016**, *45*, 237–245.
[16] Y. Zhao, R. R. Lunt, *Adv. Energy Mater.* **2013**, *3*, 1143–1148.
[17] a) M. Robin, W. Kuai, M. Amela-Cortes, S. Cordier, Y. Molard, T. Mohammed-Brahim, E. Jacques, M. Harnois, *ACS Appl. Mater. Interfaces* **2015**, *7*, 21975–21984; b) Y. Molard, C. Labbe, J. Cardin, S. Cordier, *Adv. Funct. Mater.* **2013**, *23*, 4821–4825; c) M. Amela-Cortes, A. Garreau, S. Cordier, E. Faulques, J.-L. Duvail, Y. Molard, *J. Mater. Chem. C* **2014**, *2*, 1545–1552; d) M. Robin, N. Dumait, M. Amela-Cortes, C. Roiland, M. Harnois, E. Jacques, H. Folliot, Y. Molard, *Chem. Eur. J.* **2018**, *24*, 4825–4829.
[18] J. A. Jackson, C. Turro, M. D. Newsham, D. G. Nocera, *J. Phys. Chem.* **1990**, *94*, 4500–4507.
[19] a) R. N. Ghosh, G. L. Baker, C. Ruud, D. G. Nocera, *Appl. Phys. Lett.* **1999**, *75*, 2885–2887; b) M. Amela-Cortes, S. Paofai, S. Cordier, H. Folliot, Y. Molard, *Chem. Commun.* **2015**, *51*, 8177–8180.
[20] N. Brandhonneur, T. Hatahet, M. Amela-Cortes, Y. Molard, S. Cordier, G. Dollo, *Eur. J. Pharm. Biopharm.* **2018**, *125*, 95–105.
[21] A. Ledneva, S. Ferlay, N. G. Naumov, M. Mauro, S. Cordier, N. Kyritsakas, M. W. Hosseini, *New J. Chem.* **2018**, *42*, 11888–11895.
[22] N. Sinha, L. Stegemann, T. T. Y. Tan, N. L. Doltsinis, C. A. Strassert, F. E. Hahn, *Angew. Chem. Int. Ed.* **2017**, *56*, 2785–2789.
[23] A. S. Pronin, S. S. Yarovoy, Y. M. Gayfulin, A. A. Ryadun, K. A. Brylev, D. G. Samsonenko, I. V. Eltsov, Y. V. Mironov, *Molecules* **2020**, *25*, 5796.
[24] Deposition Numbers CCDC 2320723 and CCDC 2320491 contain the supplementary crystallographic data for this paper. These data are provided free of charge by the joint Cambridge Crystallographic Data Centre and Fachinformationszentrum Karlsruhe Access Structures service.
[25] a) J. Rouillon, C. Monnereau, C. Andraud, *Chem. Eur. J.* **2021**, *27*, 8003–8007; b) M. de la Hoz Tomás, M. Yamaguchi, B. Cohen, I. Hisaki, A. Douhal, *Phys. Chem. Chem. Phys.* **2023**, *25*, 18874–18888.
[26] D. A. Shultz, M. A. Fox, *J. Am. Chem. Soc.* **1989**, *111*, 6311–6320.
[27] a) S. Khlifi, N. Fournier Le Ray, S. Paofai, M. Amela-Cortes, H. Akdas-Kilic, G. Taupier, S. Derien, S. Cordier, M. Achard, Y. Molard, *Mater. Today* **2020**, *35*, 34–41; b) S. Khlifi, J. Bigeon, M. Amela-Cortes, N. Dumait, H. Akdas-Kiliç, G. Taupier, S. Freslon, S. Cordier, S. Derien, M. Achard, G. h. Loas, Y. Molard, *J. Mater. Chem. C* **2021**, *9*, 7094–70102.
[28] K. Kirakci, M. A. Shestopalov, K. Lang, *Coord. Chem. Rev.* **2023**, *481*, 215048.
[29] N. S. Makarov, M. Drobizhev, A. Rebane, *Opt. Express* **2008**, *16*, 4029–4047.
[30] S. Khlifi, G. Taupier, M. Amela-Cortes, N. Dumait, S. Freslon, S. Cordier, Y. Molard, *Inorg. Chem.* **2021**, *60*, 5446–5451.
[31] J. R. Lakowicz, in *Principles of Fluorescence Spectroscopy*, third edition, Springer, Boston, MA, **2006**.

Manuscript received: January 25, 2024
Accepted manuscript online: January 29, 2024
Version of record online: February 19, 2024